Published by IOP Publishing for Sissa Medialab
Received: *December 9, 2016*
Revised: *January 23, 2017*
Accepted: *February 16, 2017*
Published: *???, 2017*

Characterisation of a CZT detector for dosimetry of molecular radiotherapy

L.H. McAreavey,[a,1] **L.J. Harkness-Brennan,**[a] **S.J. Colosimo,**[a] **D.S. Judson,**[a] **A.J. Boston,**[a] **H.C. Boston,**[a] **P.J. Nolan,**[a] **G.D. Flux,**[b] **A.M. Denis-Bacelar,**[c] **B. Harris,**[d] **I. Radley,**[e] **and M. Carroll**[f]

[a] *The Oliver Lodge Laboratory, University of Liverpool, Liverpool, L69 7ZE, U.K.*
[b] *The Royal Marsden Hospital, Sutton, SM2 5PT, U.K.*
[c] *The Institute of Cancer Research, Sutton, SM2 5NG, U.K.*
[d] *eV Products Inc. (Kromek U.S.A.), Saxonburg, PA 16056, U.S.A.*
[e] *Kromek Group plc, Sedgefield, TS21 3FD, U.K.*
[f] *The Royal Liverpool and Broadgreen University Hospital, Liverpool, L7 8XP, U.K.*

E-mail: lhm@ns.ph.liv.ac.uk

Abstract: A pixelated cadmium zinc telluride (CZT) detector has been characterised for the purpose of developing a quantitative single photon emission computed tomography (SPECT) system for dosimetry of molecular radiotherapy (MRT). This is the aim of the Dosimetric Imaging with CZT (DEPICT) project, which is a collaboration between the University of Liverpool, The Royal Marsden Hospital, The Royal Liverpool and Broadgreen University Hospital, and the commercial partner Kromek. CZT is a direct band gap semiconductor with superior energy resolution and stopping power compared to scintillator detectors in current SPECT systems. The inherent detector properties have been investigated and operational parameters such as bias voltage and peaking time have been selected to optimise the performance of the system. Good energy resolution is required to discriminate γ-rays that are scattered as they are emitted from the body and within the collimator, and high photon throughput is essential due to the high activities of isotopes administered in MRT. The system has an average measured electronic noise of 3.31 keV full width at half maximum (FWHM), determined through the use of an internal pulser. The energy response of the system was measured across the energy region of interest 59.5 keV to 364.5 keV and found to be linear. The reverse bias voltage and peaking time producing the optimum FWHM and maximum photon throughput were 600 V and 0.5 μs respectively. The average dead time of the system was measured as 4.84 μs and charge sharing was quantified to be 0.71 % at 59.5 keV. A pixel sensitivity calibration map was created and planar images of the medical imaging isotopes ^{99m}Tc and ^{123}I were acquired by coupling the device to a prototype collimator, thereby demonstrating the suitability of the detector for the DEPICT project.

Keywords: Gamma camera, SPECT, PET PET/CT, coronary CT angiography (CTA); Gamma detectors (scintillators, CZT, HPG, HgI etc); Radiotherapy concepts; Solid state detectors

[1] Corresponding author.

doi:xxxxxxx

Contents

1 Introduction

Molecular radiotherapy (MRT) involves the internal administration of radiopharmaceuticals to deliver high absorbed doses to targeted tumour tissue whilst minimising the dose to surrounding healthy tissue. Although MRT has been used clinically for around 75 years [1], there are no standardised dosimetry practices to calculate the absorbed dose delivered to tumour targets or organs at risk from the administered activity. Current MRT treatment plans are undesirably generic as the administered activity is often fixed for a given procedure or scaled according to the weight or body surface area of the patient [2]. However, the uptake and retention of the MRT therapeutic agents and hence the absorbed dose can vary by up to two orders of magnitude between patients [3, 4] due to the wide range of biokinetics and disease status. The outcome of the treatment is therefore somewhat uncertain and can lead to unnecessary expense.

MRT utilises a radionuclide that emits charged particles, as their high linear energy transfer causes damage to local cells. For dosimetry purposes, γ-rays are also emitted that can be detected to track the biodistribution of activity. This is currently achieved with scintillation imaging such as single photon emission computed tomography (SPECT) [5]. However, quantitative information is sometimes lost in current diagnostic SPECT systems due to dead time as they are not optimised for the levels of activity administered in MRT, which can typically range from 3.7–10 GBq [6]. The high activities cause large count losses, which entail an underestimation of the doses received by

organs, and therefore it is essential to correct for this effect in dosimetric studies [7]. The challenge with image quantification is exacerbated by the fact that current gamma cameras are optimised for use with low energy diagnostic imaging isotopes, mainly ^{99m}Tc (140.5 keV γ-ray), rather than higher energy therapeutic isotopes, such as ^{131}I (364.5 keV γ-ray). Therefore, a custom-designed compact SPECT system is being developed to facilitate quantitative imaging for MRT based on a collimated, pixelated, cadmium zinc telluride (CZT) detector. This is the aim of the Dosimetric Imaging with CZT (DEPICT) project, which is a collaboration between the University of Liverpool, The Royal Marsden Hospital, The Royal Liverpool and Broadgreen University Hospital and the commercial partner Kromek. The system will facilitate real-time assessment of the absorbed dose delivered to the patient, which may then be tailored specifically for MRT of the thyroid using an ^{131}I tracer. CZT is a room temperature, direct band gap semiconductor with superior energy resolution, spatial resolution and stopping power compared to conventional scintillator based SPECT detector systems [8]. These favourable physical characteristics have led to considerable research on the use of CZT detectors in nuclear medicine [9].

There are three interlinking work packages in the DEPICT project: optimisation of the detector, and the development of a custom-designed high-energy collimator suitable for use with ^{131}I and appropriate SPECT reconstruction algorithms, to visualise the 3-dimensional distribution of the radiopharmaceutical in the body to obtain quantitative activity information. The aims of the detector optimisation work package are to:

- Optimise and evaluate detector performance
- Quantify dead time, to input to collimator design criteria
- Provide a pixel sensitivity calibration map, as input for the reconstruction algorithm
- Produce planar images for preliminary performance evaluation

This paper outlines the experimental methods used to achieve these aims and evaluates the results.

2 Detector system

The DMatrix Nuclear Imager manufactured by Kromek, shown in figure 1, is a fully integrated, photon counting, pixelated, 12-bit energy discriminating CZT detector with modular design that enables large field of view scaling [10]. Its end-user applications include gamma spectroscopy for nuclear security and as a SPECT demonstrator in the medical industry. It consists of four CZT detector modules, each coupled to an application specific integrated circuit (ASIC) to process and read out the signals, ADC converters, and an aggregator field programmable gate array (FPGA). Each detector module is $22 \times 22 \times 5$ mm with 11×11 pixels at 2 mm pitch. Each ASIC has 128 anode channels (121 used) for anode pixels and 2 cathode channels (1 used) performing charge amplification and shaping, and providing both energy and timing information. Both the anode and cathode channels utilise a charge sensitive preamplifier with adaptive reset, a 5^{th} order unipolar shaping amplifier, baseline stabiliser and discriminator with trimming. After shaping, the analog outputs of the ASIC are digitized. The aggregated 2×2 units communicate with a master FPGA

over a low-voltage differential signaling (LVDS) tether, where the data is formed into packets. The packets are received by a PC where the DMatrix API decodes them, and presents the end user with list-mode data. Suitable software is then used to view this list-mode data as a γ-ray energy spectrum. For the 2×2 configuration, Gigabit Ethernet is sufficient for communication with a PC. A carbon fiber window covers the active area of the detector at a height of 1.36 cm from the closest face of the detector, and this can be removed to allow a mechanical collimator to be mounted. The CZT detectors and associated electronics are encased in aluminium to allow shielding from visible light, which would otherwise induce noise.

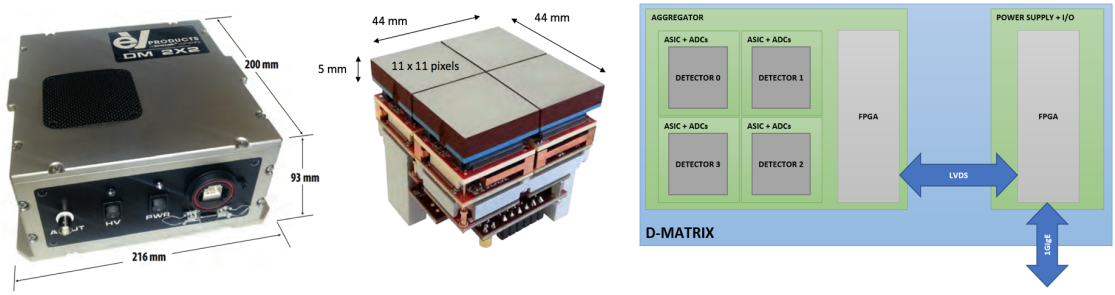

Figure 1. DMatrix external housing, 4 CZT detector modules and simplified block diagram [10].

3 Optimising CZT detector performance

Measurements were taken to optimise and evaluate the performance of the CZT detector for MRT to determine settings that facilitate both good energy resolution and high photon throughput. Unless otherwise stated, throughout the investigation the reverse bias voltage was set at the recommended operating voltage of 600 V and internal cooling fans were switched on to stabilise the temperature of the electronics, which has been shown to prevent photopeak drift. The basic sparsified photon collection mode was used, which entails only collecting data from the anode channels that exceed a user-defined threshold. For a pixel to trigger the data read out, its voltage pulse height must be greater than the threshold set in mV for that pixel, which is adjustable by a 10-bit DAC. A global threshold sets the same value for all pixels, and a threshold of 380 mV was applied, calculated to be equivalent to ~15 keV. The threshold was used to remove electronic noise contributions at low energy.

3.1 Electronic noise

An internal digital test pulser was used to estimate the electronic noise contribution to the total energy resolution, allowing noise contributions from charge production and collection to be excluded. Pulser circuitry is internal to the ASIC and charge is injected to the front of the preamplifier. The pulser amplitude is controlled by a 10-bit DAC in the ASIC. A test pulse of amplitude 52.86 mV was induced for 60 seconds, allowing a peak in each pixel to be produced with approximately 45,000 gross counts. Overall, the system had an average measured electronic noise of 3.31 ± 0.24 keV FWHM. Electronic noise of around 3 keV in pixelated CZT detectors have been reported in [11, 12].

3.2 Operating voltage

Measurements were made at reverse bias voltages between 300 V to 1000 V, in steps of 100 V, to determine the voltage that produced the best energy resolution of an ^{131}I 364.5 keV photopeak. The peak fitting programme GF3 [13] was utilised to apply a skewed Gaussian fit to the photopeak, of which an example is shown in figure 2a. The two smooth lines show the total fit to a 364.5 keV photopeak and the background fit. The residual plot indicating the difference between the data and the fit is also illustrated by the irregular line across the x-axis. A skewed Gaussian fit is required due to low energy tailing, which is characteristic of incomplete charge collection in the CZT detector due to hole trapping [14, 15]. The data plotted in figure 2b shows an average energy resolution (FWHM %) of the 364.5 keV photopeak calculated by noting the FWHM and photopeak centroid position from a typical pixel from each detector module and calculating the average FWHM (%) value, at each bias voltage. The experimental data has a fit of the form:

$$f(x) = 281.8 \cdot e^{(-0.01x)} + 1.9 \cdot e^{(0.0006x)} \tag{3.1}$$

The results presented in figure 2b demonstrate that as the voltage is increased from 300V to 600V, the FWHM (%) decreases from 7.8 % to 2.9 %, due to improved charge collection. However, as the bias voltage is increased above 600 V, the FWHM (%) degrades due to increasing leakage current. Therefore 600 V was selected as the optimum reverse bias voltage for operation.

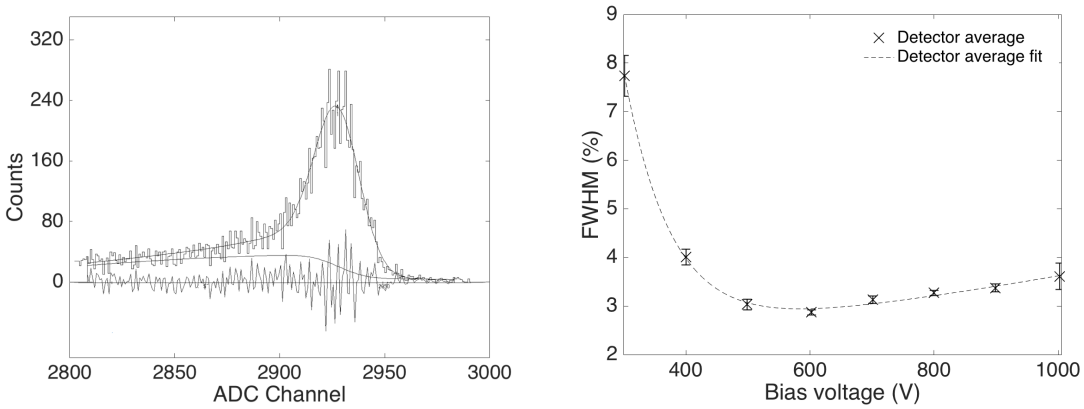

Figure 2. (a) 364.5 keV ^{131}I photopeak illustrating appropriate skewed Gaussian fit. (b) Detector average FWHM (%) values calculated for the ^{131}I 364.5 keV photopeak as a function of bias voltage.

3.3 Detector linearity

Data were acquired with ^{241}Am (59.5 keV γ-ray, 179.5 kBq), ^{133}Ba (81, 356 keV γ-rays, 138.9 kBq), ^{57}Co (122 kev γ-ray, 343.3 kBq) and ^{139}Ce (165.9 keV γ-ray, 26.4 kBq) point sources and an ^{131}I (364.5 keV γ-ray, ~8 MBq) distributed source to determine if the detector and associated electronics were linear in energy response. The energy range provided by these sources [16, 17] corresponds to the current energy region of interest in the DEPICT project. The gain on the anode channel can

be set to one of four values in the ASIC; 20 mV/fC, 40 mV/fC, 60 mV/fC and 120 mV/fC, so these were investigated to maximise the use of the dynamic range. The sources were sequentially placed 4 cm from the carbon fiber window for 600 seconds at each gain setting.

Figure 3a shows the ADC channel number of the measured photopeak centroid plotted as a function of known γ-ray energy for all the acquired data sets. It can be seen that the energy response is linear below 364.5 keV for all gain settings. A linear calibration was therefore applied across the energy range. Figure 3a shows the intercept at ADC channel 500, which is due to a baseline offset of 230 mV in the pulses. The dynamic range was known to be approximately 2 V from this baseline and the total range consists of 4096 channels. The 120 mV/fC setting is optimum in this energy region as the data best fills the dynamic range, and will be used in remaining measurements. Therefore the % deviation of the measured ADC channel from the ADC channel calculated from the linear fit for the 120 mV/fC data is plotted in figure 3b. The measured ADC channel numbers for all energies are within ± 0.5 % of the calculated ADC channel numbers. The maximum theoretical energy that can be resolved at this gain setting has been calculated to be 558 keV, however it is unlikely that the detector would have suitable efficiency at detecting γ-ray energies above 364.5 keV due to the 5 mm crystal thickness.

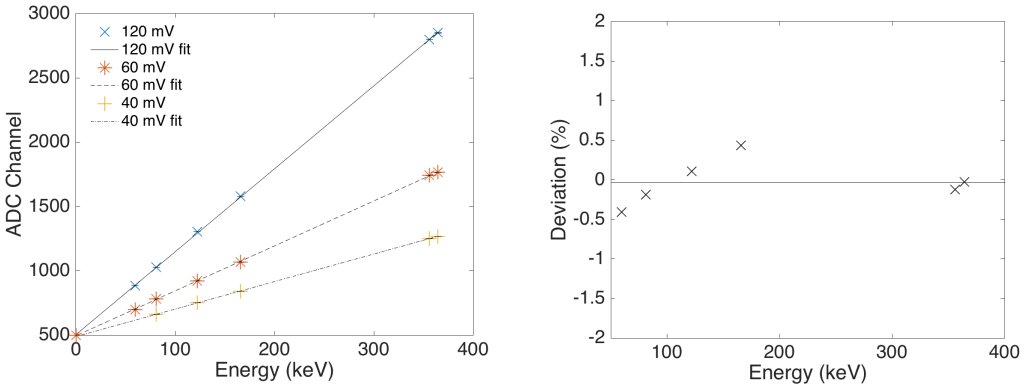

(a) **(b)**

Figure 3. (a) Plot of photopeak ADC channel as a function of known γ-ray energy. (b) % deviation of measured photopeak ADC channel from ADC channel calculated from the linear fit, at 120 mV/fC.

3.4 Peaking time

To determine the energy of an incident photon, the voltage pulse produced by the detector must be shaped. The amount of shaping depends on the peaking time, illustrated in figure 4a. Four peaking time values can be set by the user in the ASIC; 0.25, 0.5, 1.0 and 2.0 μs. The energy resolution (FWHM %) of an ^{131}I 364.5 keV photopeak from a single pixel was measured to be 8.66 ± 0.05 %, 2.94 ± 0.02 % and 4.56 ± 0.21 % at peaking times of 0.25, 0.5, and 1.0 μs respectively. At 2.0 μs peaking time, the photopeak was no longer resolvable. It is known that lowering the threshold helps to recover the spectrum at the longer peaking time, although this is not desirable for the high-count rate application of DEPICT. The best energy resolution of 2.94 ± 0.02 % was observed at a peaking time of 0.5 μs. An example ^{131}I spectrum acquired at this peaking time is shown in figure 4b with

the photopeak centroids labeled. The 80.2 keV (P_γ = 2.6 %), 284.3 keV (P_γ = 6.1 %) and 364.5 keV (P_γ = 81.5 %) ^{131}I photopeaks are clearly identified. There are multiple unresolvable low energy x-rays with energies between 29.5–34.5 keV, and a combined intensity of 4.86 %. For comparison, a typical energy resolution for NaI (Tl) scintillator detectors currently used in SPECT systems is ~10 % FWHM at 364.5 keV. The superior CZT detector energy resolution will facilitate improved scatter correction over scintillation SPECT systems, improving quantitative imaging and volume delineation, which are key aims of the DEPICT project.

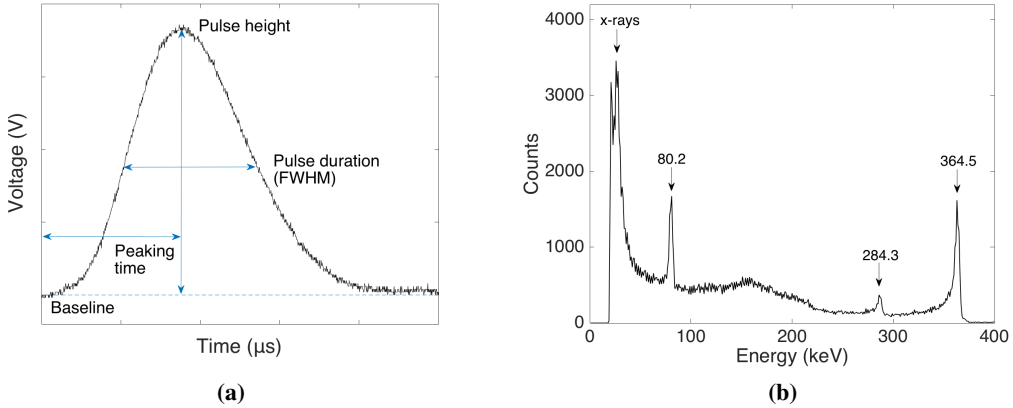

(a) **(b)**

Figure 4. (a) Illustration of a shaped preamplifier pulse to define peaking time, pulse height and pulse duration. (b) An example ^{131}I energy spectrum acquired at 0.5 μs peaking time.

The setup parameters of bias voltage and peaking time have been selected so far to optimise energy resolution for good discrimination of scattered γ-rays. However, the DEPICT project also requires the detector to operate with high photon throughput, due to the high activities of isotopes administered in MRT. This could potentially be achieved by reducing the peaking time. Therefore, the photon throughput was compared at peaking times of 0.25 and 0.5 μs. The detector was exposed to a 3.54 MBq ^{133}Ba point source for measurement periods of 300 seconds, at a range of distances from 0 cm (on the carbon fiber window) to 14 cm, to vary the incident count rate. The incident count rate was calculated using the activity of the source, the time taken for data collection and a solid angle, Ω, correction for a square detector shown in equations. (3.2) and (3.3), at each distance.

$$\Omega = (1 - f_s) \cdot 4 \cdot \arcsin\left(\sin^2 \alpha\right) \tag{3.2}$$

where

$$\alpha = \arctan\left(\frac{w}{2d}\right) \tag{3.3}$$

and where f_s is an pre-factor to account for any physical shadowing of the detector area by ancillary windows, w is the active width of the detector and d is the distance from the detector to the source [18]. The ^{133}Ba point source emits a 356 keV γ-ray, an analogue to the 364.5 keV ^{131}I γ-ray, and was used for this measurement due to the uncertainties that would arise in the solid angle correction to be applied to the ^{131}I distributed source. The total measured count rate was recorded and shown as a function of the incident count rate for the data acquired for peaking times of 0.25 and 0.5 μs in figure 5.

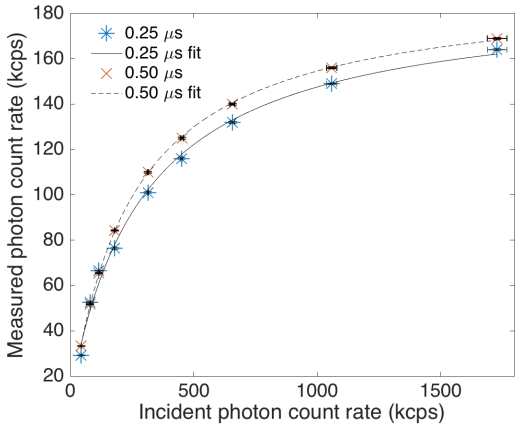

Figure 5. Measured photon count rate as a function of incident photon count rate at peaking times of 0.25 μs and 0.5 μs.

These results show shortening the peaking time to 0.25 μs slightly decreased the photon throughput, which may be due to ballistic deficit effects. The error on the measured photon count rate is statistical, whereas the error on the incident count rate takes into account geometrical uncertainties. Since the peaking time is not the limiting factor for throughput, the detector could therefore be operated at 0.5 μs to ensure best spectroscopic performance.

4 Dead time

The dead time of a SPECT system has always been a main limitation for quantitative imaging in MRT and it is therefore essential to minimise the effect where possible. It can be seen in figure 5 that the relationship between the incident and measured count rates is non-linear. If the gradient of the graph is non-zero, it is possible to apply a dead time correction. However, it is seen that the data begins to plateau around 160×10^3 measured photon counts per second, which indicates the incident count rate can no longer be calculated from the known relationship to the measured count rate, and dead time corrections can no longer be used. This maximum operating count rate of 160 kcps is in agreement with the manufacturers specifications and will be used to determine the transmission required from the custom-designed DEPICT collimator.

The two-source method [19] was used with 3.54 MBq and 0.95 MBq ^{133}Ba point sources at the optimised peaking time of 0.5 μs, to determine the system dead time. Count rates were measured when the sources were placed at heights of 4 cm and 8 cm above the carbon fiber window, for 600 seconds. A background measurement was also acquired. The dead time, τ, of the system can be calculated from the following two-source method equation:

$$\tau = \frac{X(1 - \sqrt{1 - Z})}{Y} \tag{4.1}$$

where

$$X \equiv m_1 m_2 - m_b m_{12} \tag{4.2}$$

$$Y \equiv m_1 m_2 (m_{12} + m_b) - m_b m_{12} (m_1 + m_2) \tag{4.3}$$

$$Z \equiv \frac{Y(m_1 + m_2 - m_{12} - m_b)}{X^2} \tag{4.4}$$

and where m_1 = measured count rate of source 1, m_2 = measured count rate of source 2, m_{12} = measured count rate of sources 1 and 2 combined and m_b is a measure of the background counts. The values for m_1, m_2, m_{12}, m_b and τ at each height are shown in table 1. The average dead time was calculated to be 4.84 ± 0.05 μs.

Table 1. Values used for calculation of dead time.

Height (cm)	m_1 (cps)	m_2 (cps)	m_{12} (cps)	m_b (cps)	τ (μs)	Error (μs)
4	1.08×10^5	4.99×10^4	1.21×10^5	3.29×10^1	4.80	0.07
8	6.43×10^4	2.36×10^4	8.80×10^4	3.29×10^1	4.87	0.08

5 Pixel sensitivity calibration

In order to extract quantitative information from the DEPICT SPECT images, it is necessary to calibrate the position-dependent sensitivity of the CZT detector and the collimator. In this phase of work, the CZT detector sensitivity has been calculated for each pixel, so that a pixel sensitivity calibration map can be input to the image reconstruction algorithms, which are currently under development. A 1.64 GBq ^{241}Am source collimated by lead into a 1 mm beam, was mounted on a Velmex VXM x-y positioning table 1.5 cm above the carbon fiber window, to acquire data for γ-rays incident on the detector at known x-y positions, as shown in figures 6a and 6b. The collimated source was moved across the face of the detector in an x-y grid. The step between collimator positions was set at 1 mm and data collected for 10 seconds at each position. The optimised bias voltage of 600 V, gain setting of 120 mV/fC and peaking time of 0.5 μs were set for data acquisition.

(a) **(b)**

Figure 6. (a) Photograph of the CZT detector and collimated ^{241}Am source mounted on the Velmex scanning table. (b) Photograph of the end of the collimator. The collimated γ-rays are incident on the carbon fiber entrance window.

Figure 7a shows a plot of the total counts in the detector recorded as a function of x-y grid scan position. Figure 7a shows the four separate gamma modules are easily discernible, however the modules are not accurately aligned with one another. It was observed that detector modules 3 and 0 have approximately 11 % more counts, with respect to modules 2 and 1. The yellow areas of

reduced intensity, approximately 3500 counts per position, arise due to the diverging photon beam interacting with the detector module edge pixels, when the collimated source was positioned over the gap between the modules. The black pixel in module 1 is due to an issue in the software that stopped data collection at 1 scan position, and the dark blue pixels of approximately 1000 counts in module 0 highlight two defective pixels. The pixels surrounding the two defective pixels also have reduced counts, due to the photon beam diverging as it leaves the end of the collimator and counts being lost in the defective pixels.

An energy gated plot is shown in figure 7b with an energy gate of 52–62 keV applied around the 59.5 keV ^{241}Am photopeak. It highlights degradation of the outer pixels, predominantly in module 3, showing that less events have been detected. It is expected this is due to poor charge collection. Comparison of the ^{241}Am energy spectra obtained from an inner module pixel and a degraded edge pixel from detector module 3 are shown in figure 7c, and the spectrum from the edge pixel has a poorer peak-to-total ratio. Edge pixels can degrade due to environmental effects, and also due to light passing through gaps in the aluminium case, inducing noise. The pixel sensitivity maps will be used to calibrate future imaging data sets through normalisation of the count rate. They will allow pixel-by-pixel activity quantification, that will be input to dosimetry calculations.

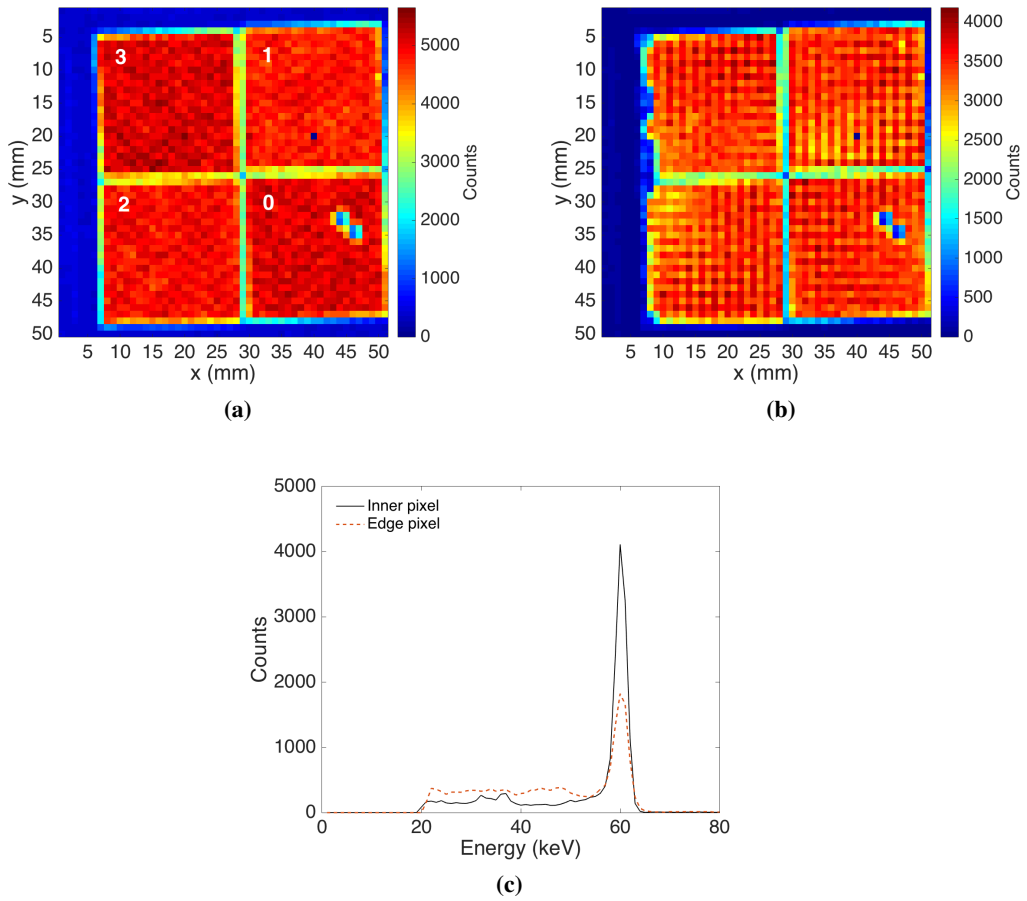

Figure 7. (a) A plot of total counts as a function of x-y position of a collimated ^{241}Am source and (b) a plot of photopeak gated counts as a function of x-y position of a collimated ^{241}Am source. (c) Comparison of ^{241}Am energy spectra from an inner module pixel and a degraded edge pixel.

6 Charge sharing

Pixelated CZT detectors allow increased spatial resolution compared to planar detectors, and this effect improves as the pixel size decreases due to the small pixel effect [20]. However, when the pixel size is decreased to be comparable to the size of the electron charge cloud created when the γ-ray interacts, the charge may be shared between multiple pixels and degrade the spatial resolution. To quantify the amount of charge sharing in the DMatrix system, a 1.64 GBq ^{241}Am source collimated into a 1 mm beam was mounted on the Velmex VXM x-y positioning table, 1.5 cm above the carbon fiber window. The step between collimator positions was set at 1 mm and data were collected for 1 second at each step. For this data collection, the readout mode was changed from the basic sparsified photon collection mode used thus far, that only read out triggered channels above a threshold, to readout all mode. This meant that any event above the set global threshold of ~15 keV would trigger the readout of all events in that detector module.

Multiple pixel events can occur either due to the aforementioned charge sharing phenomena, or because the γ-ray Compton scatters from one pixel into another, where it deposits its remaining energy. Therefore it was essential to read out the data from all pixels, in order to observe low energy Compton scattering or charge shared events that occur, with energy below 15 keV. The relative cross sections for Compton scattering and photoelectric absorption interactions by a 59.5 keV γ-ray are 0.116 cm^2/g (2.13 %) and 5.315 cm^2/g (97.86 %) respectively, for a total attenuation cross section of 5.431 cm^2/g [21]. To discriminate between charge shared and Compton scattered events, the Compton scattering formula given in equation (6.1) was used to determine the allowed energies of the scattered photon E_f and recoil electron, given the incident γ-ray had energy E_0 = 59.5 keV and the rest mass equivalent energy of the electron m_0c^2 = 511 keV.

$$E_f = \frac{E_0}{1 + \frac{E_0}{m_0c^2}(1 - \cos\theta)} \tag{6.1}$$

The range of allowed energies was calculated to be 0–11.3 keV for the energy absorbed by the electron and 48.3–59.5 keV for the scattered γ-ray, for values of θ between 0 and 180°. The lowest energy for the scattered photon results when it emerges at 180° with respect to its original direction. Therefore, any multiple pixel event, with energy outside these limits would be tagged as a charge shared event. Since the detector was in readout all mode, all pixels will have a voltage value corresponding to the collection of real charge, or due to electronic noise. Figure 8a shows an example energy spectrum acquired with the ^{241}Am source. As a result of the read out mode, a large amount of low energy noise below ~10 keV is exhibited due to background noise events being summed every time a γ-ray interacts with energy greater than 15 keV. Therefore, a threshold of 5 keV was set in post processing when quantifying the charge shared events, to discriminate some noise events. It is known however that this threshold will also remove a proportion of Compton scattered and charged shared events, with an energy less than 5 keV. The criteria for a multiple pixel event to be classed as a charge shared event is as follows:

- Energy deposited is outside Compton scatter limits
- Energy is above the post processing threshold of 5 keV

- Energy is deposited in neighbouring pixels
- Energy is deposited in the same time stamp
- Sum of energy deposited in pixel 1 and pixel 2 is less than or equal to 59.5 keV

A 2D energy spectrum is shown in figure 8b, which depicts the energy recorded in each pixel, for events in which 2 pixels pass the threshold in the same time stamp. The applied threshold of 5 keV is evident due to the lack of data below 5 keV on both the x and y axis. The red areas of counts 16,000 at 59.5 keV for both pixels corresponds to a 59.5 keV γ-ray being detected in coincidence with noise of energy between ~5–8 keV. A straight diagonal line between these regions would demonstrate Compton scattering between the two pixels, with the energy in each pixel summing to give 59.5 keV. Since there is curvature of the data, it illustrates the Compton scatter events do not have 100 % efficient charge collection, likely due to charge being trapped in the gap between the pixels [22]. There is also a small concentration of data points at 59.5, 59.5 keV, corresponding to a coincidence event where two 59.5 keV γ-rays were detected simultaneously in the two pixels.

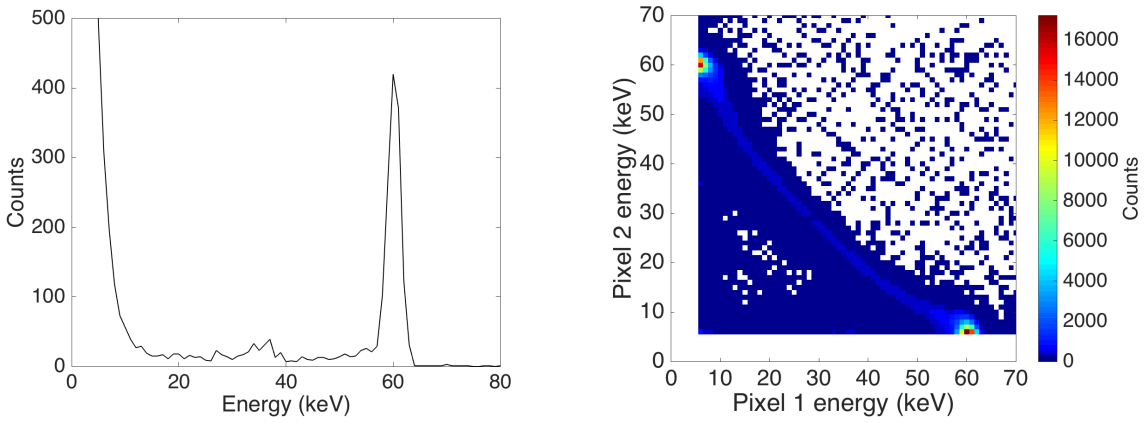

Figure 8. (a) ^{241}Am energy spectrum acquired in readout all mode, illustrating low energy noise. (b) 2D energy spectrum depicting the energy recorded in each pixel, for events in which 2 pixels pass the threshold in the same time stamp. Only data below 70 keV is included.

Following the application of the charge shared selection criteria, at 59.5 keV the ratio of charge shared events to all γ-ray interactions was determined to be 0.71 %. This is the minimum contribution of charge sharing as some events have been lost with the post processing threshold. This methodology for quantifying charge sharing is not applicable with ^{131}I, as the allowed energies for the scattered γ-ray and recoil electron are 150.2–364.5 keV and 0–214.3 keV respectively. The allowed energies of the electron and scattered γ-ray overlap, therefore the charge shared events cannot be distinguished from Compton scatter events. This is further complicated by the large increase in Compton scattering cross section by a 364.5 keV γ-ray which is 0.083 cm^2/g (72.81 %) for a total attenuation cross section of 0.114 cm^2/g [21].

7 Planar images

Data were acquired to observe imaging capability, as this is the required purpose of the CZT detector for the DEPICT project. A prototype parallel hole collimator optimised for use with 140.5 keV γ-rays was coupled to the detector to produce experimental planar images with the medical imaging isotopes ^{99m}Tc (140.5 keV γ-ray, $t_{1/2}$ = 6.01 hours) and ^{123}I (159 keV γ-ray, $t_{1/2}$ = 13.27 hours). The lead collimator was designed with hexagonal holes of size 1.2 mm, septa thickness 0.2 mm and length 23 mm. Data were acquired simultaneously with six 8 mm inner diameter vials of length 4.5 cm, filled with aqueous ^{123}I and ^{99m}Tc solutions, placed in the 6 spaces of a custom-designed Perspex phantom highlighted in figure 9a. Data were collected for 30 minutes. Figure 9b illustrates a cross sectional schematic of the position of each isotope in these 6 vials.

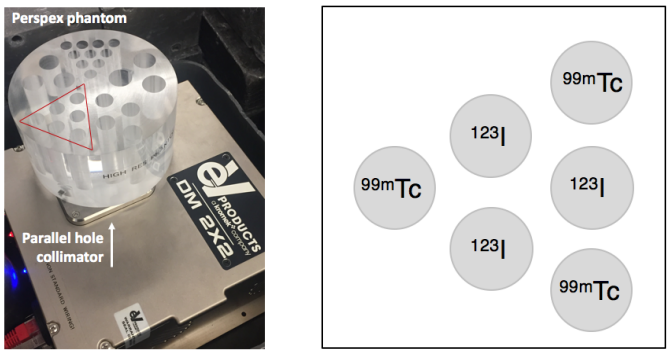

(a) **(b)**

Figure 9. (a) Photograph of the phantom positioned above the parallel hole collimator and (b) phantom schematic illustrating positions of 3 vials of ^{123}I and 3 vials of ^{99m}Tc.

The total activities of the ^{123}I and ^{99m}Tc sources were calibrated at the Royal University Liverpool Hospital, on the morning of measurement. The sources were dispensed into the 6 vials with an activity at the time of data collection of ~300 kBq and ~200 kBq in the ^{123}I and ^{99m}Tc vials, respectively. Uncertainties in the activities arise due to calibration and dispensing methods. The total energy reconstructed across all pixels within the trigger time window was calculated. This corresponds to the total energy deposited by the γ-rays in the detector system. The associated addback energy spectrum acquired with the 6 vials simultaneously, is shown in figure 10a. The FWHM of the ^{99m}Tc and ^{123}I photopeaks were measured to be 7.2 keV and 7.4 keV respectively, and the peaks are clearly resolvable, demonstrating the good energy resolution of CZT. For comparison, a typical value for the energy resolution of a 140.5 keV photopeak with a scintillator detector is ~14 keV FWHM [23]. The two peaks at approximately 75 and 85 keV correspond to lead x-rays produced in fluorescence from the collimator. Figure 10b illustrates the pixel intensity map produced, for events with energy between 130 and 170 keV to encompass the photopeaks of both sources, whilst reducing contributions from scattered γ-rays. This energy gate is indicated in red in figure 10a.

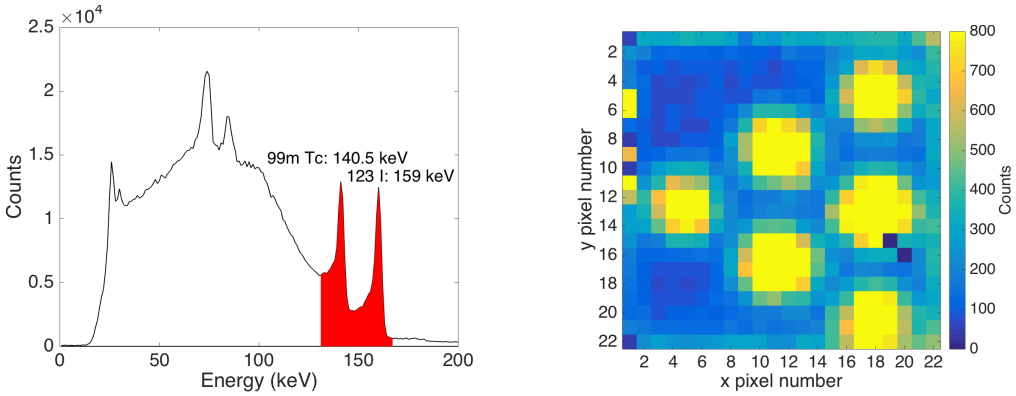

(a) (b)

Figure 10. (a)The addback energy spectrum corresponding to the total energy reconstructed across all pixels within the trigger time window, with energy gate applied to (b) highlighted (b) gated pixel intensity map acquired with 3 vials of ^{123}I and 3 vials of ^{99m}Tc, positioned as per figure 9b.

Figures 11a and 12a show single pixel energy spectra selected from the pixel map regions corresponding to ^{123}I and ^{99m}Tc, respectively. Figures 11b and 12b show the corresponding energy gated intensity pixel maps of the ^{123}I and ^{99m}Tc vials, respectively. The red highlighted region on each spectrum indicates the applied energy gate to achieve the gated pixel maps; 150–165 keV for the 159 keV ^{123}I photopeak and 130–145 keV around the 140.5 keV ^{99m}Tc photopeak. The red square on the pixel map highlights which pixel the spectrum shown was obtained from.

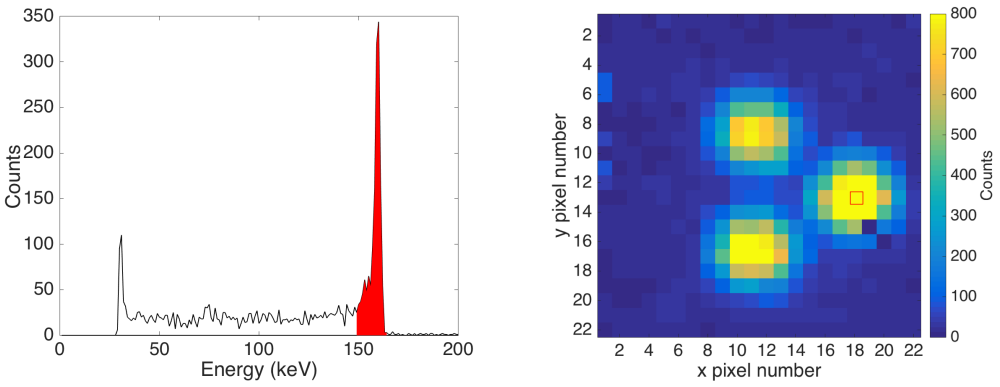

(a) (b)

Figure 11. (a) ^{123}I energy spectrum acquired from the single pixel highlighted by the red square in the pixel intensity map and (b) pixel intensity map gated on the ^{123}I 159 keV photopeak. Gate shown as solid red shaded area in (a).

It can be seen in figure 11b that when an energy gate is applied to the ^{123}I data, only the 3 rods filled with ^{123}I are visible. However, even though a background subtraction has been applied, figure 12b exhibits regions of intensity of approximately 100 counts above background on the ^{99m}Tc gated pixel map where the ^{123}I rods are known to be. Although the energy gate is applied around the ^{99m}Tc photopeak, it sits on the Compton background of ^{123}I, demonstrated in figure 10a. Therefore

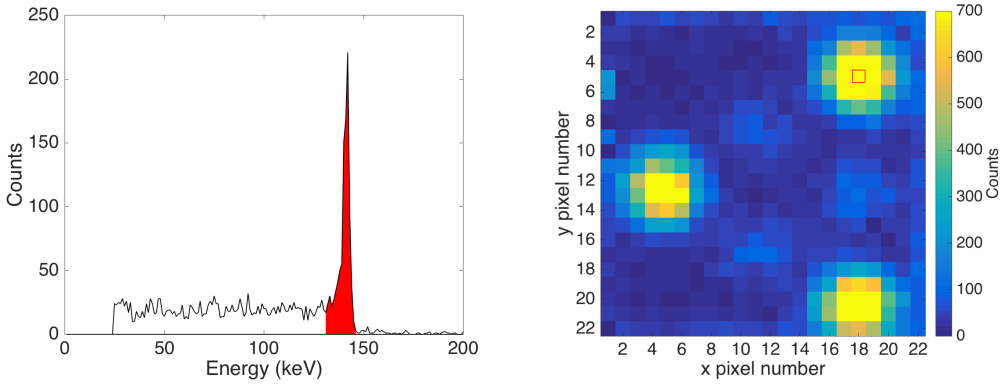

Figure 12. (a) ^{99m}Tc energy spectrum acquired from the single pixel highlighted by the red square in the pixel intensity map and (b) pixel intensity map gated on the ^{99m}Tc 140.5 keV photopeak. Gate shown as solid red shaded area in (a).

events in the ^{99m}Tc pixel map arise from ^{123}I emissions, but at ~15 % of the rate of observed ^{99m}Tc counts. It was not possible to perform a detailed quantitative analysis due to the uncertainties in known vial activities. The results however do use multi-isotope imaging to demonstrate the power of discriminating events by detected γ-ray energy in the CZT detector, which will be important for rejecting events scattered within the patient and collimator during MRT.

Improving volume delineation in SPECT is an important aim of the DEPICT project. In order to determine the accuracy of deducing the size of a vial from a planar image, an intensity profile was taken through x pixel number = 4 from the ^{99m}Tc pixel intensity map shown in figure 12b and is plotted in figure 13. This corresponds to the position of maximum inner diameter of one of the ^{99m}Tc vials, known to be 8 mm.

The fit applied to the data was a Gaussian with a quadratic background correction:

$$f(x) = a_1 e^{\left(-\left(\frac{x-b_1}{c_1}\right)^2\right)} + p1x^2 + p2x + p3. \tag{7.1}$$

The standard deviation σ of the peak was determined by $\sigma_1 = \frac{c_1}{\sqrt{2}}$ to be 1.61 ± 0.10, and was input to FWHM = $2\sqrt{2ln(2)}\,\sigma$. Therefore the FWHM of the peak is 3.80 ± 0.24 pixels. Since each pixel is 2 mm, it demonstrates the region of high intensity is 7.60 ± 0.48 mm. This is consistent with the experimental set up as the vials used had an 8 mm internal diameter. Therefore, the pixel size and prototype collimator successfully facilitate area delineation of the rods. These imaging results are the first steps towards producing tomographic images with the custom-designed collimator and reconstruction algorithms later in the DEPICT project. The excellent spatial resolution in these planar images, coupled with excellent energy discrimination underpin the future success of the project. Volume delineation will be investigated following tomographic reconstruction of planar images acquired using DEPICT.

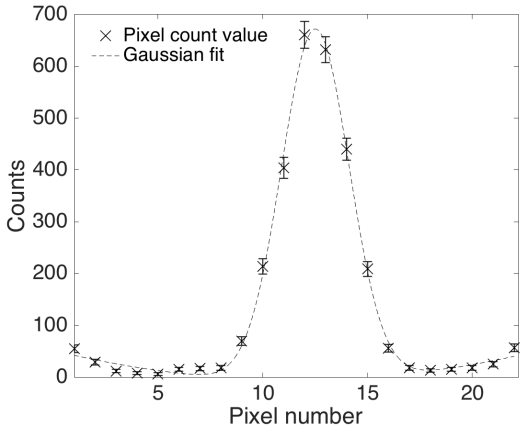

Figure 13. Profile from a slice through the ^{99m}Tc pixel intensity map at x = 4.

8 Conclusions

A pixelated CZT detector has been characterised at the University of Liverpool for application as an imaging dosimeter in MRT, for the DEPICT project. The detector has been optimised for both energy resolution and throughput with a peaking time of 0.5 μs and a reverse bias voltage of 600 V. Good energy resolution is required due to the large contribution from scattered γ-rays as they are emitted from the body, and high throughput is necessary due to the large activities administered in MRT. The average dead time was calculated to be 4.84 ± 0.05 μs, and it is possible to apply dead time corrections up to approximately 160 kcps detected count rate. Pixel sensitivity calibration maps were produced and will be used to calibrate future imaging sets through normalisation of the count rate, and allow pixel-by-pixel activity quantification. Charge sharing was investigated and 0.71 % of the γ-ray events, above a 5 keV threshold, were calculated to be charge shared events at 59.5 keV and will be corrected for. The results of this paper are being input to the design of a collimator and development of image reconstruction algorithms. The experimental characterisation demonstrates that the CZT detector is ideally suited for this particular application, due to its measured count rate capabilities, position sensitivity and energy resolution. Future work will include imaging a thyroid phantom with high activity ^{131}I to evaluate the performance of the detector in a clinical setting.

Acknowledgments

The authors wish to acknowledge financial support from the U.K. Science and Technology Facilities Council through the research award ST/M007847/1.

References

[1] S. Hertz and A. Roberts, *Radioactive Iodine in the Study of Thyroid Physiology VII. The Use of Radioactive Iodine Therapy in Hyperthyroidism*, *J. Am. Med. Assoc.* (1946) 81.

[2] D.R. McGowan and M.J. Guy, *Time to demand dosimetry for molecular radiotherapy?*, *Br. J. Radiol.* **88** (2015) 20140720.

[3] G.D. Flux et al., *A dose-effect correlation for radioiodine ablation in differentiated thyroid cancer*, *Eur. J. Nucl. Med. Mol. Imaging* **37** (2010) 270.

[4] G. Sgouros et al., *Patient-Specific Dosimetry for ^{131}I Thyroid Cancer Therapy Using ^{124}I PET and 3-Dimensional-Internal Dosimetry (3D-ID) Software*, *J. Nucl. Med.* **45** (2004) 1366.

[5] G.D. Flux et al., *The impact of PET and SPECT on dosimetry for targeted radionuclide therapy*, *Z. Med. Phys.* **16** (2006) 47.

[6] M. Lassmann, C. Reiners and M. Luster, *Dosimetry and thyroid cancer: the individual dosage of radioiodine*, *Endocr. Relat. Cancer* **17** (2010) R161.

[7] L. Ferrer et al., *Dosimetric Impact of Correcting Count Losses due to Deadtime in Clinical Radioimmunotherapy Trials Involving Iodine-131 Scintigraphy*, *Cancer Biother. Radiopharm.* **18** (2003) 117.

[8] K. Iniewski, *CZT detector technology for medical imaging*, 2014 *JINST* **9** C11001.

[9] C. Scheiber, *CdTe and CdZnTe detectors in nuclear medicine*, *Nucl. Instrum. Meth.* **A 448** (2000) 513.

[10] *Kromek: DMatrix — nuclear imager gamma spectroscopy detector/imager and software*, http://www.kromek.com/index.php/medical/all-medical-products/dmatrix.

[11] J.C. Kim et al., *Charge sharing in common-grid pixelated CdZnTe detectors*, *Nucl. Instrum. Meth.* **A 654** (2011) 233.

[12] Y. Yin, Q. Liu, D. Xu and X. Chen, *Charge sharing effect on 600 μm pitch pixelated CZT detector for imaging applications*, *Chin. Phys.* **C 38** (2014) 116002 [arXiv:1312.6766].

[13] D.C. Radford, *Radware software package*, (2000).

[14] Q. Zhang et al., *Progress in the Development of CdZnTe Unipolar Detectors for Different Anode Geometries and Data Corrections*, *Sensors* **18** (2013) 2447.

[15] A. Shor et al., *Gamma Spectroscopy With Pixelated CdZnTe Detectors*, *IEEE Trans. Nucl. Sci.* **51** (2004) 1204.

[16] M.-M. Bé et al., *Table of radionuclides, Vol.* 1 — $A = 1$ *to* 150, *Monographie BIPM-5 Bureau International des Poids et Mesures* (2004).

[17] M.-M. Bé et al., *Table of radionuclides, Vol.* 2 — $A = 151$ *to* 242, *Monographie BIPM-5 Bureau International des Poids et Mesures* (2004).

[18] N.J. Zaluzec, *Analytical Formulae for Calculations of X-ray Detector Solid Angles in the Scanning and Scanning/Transmission Analytical Electron Microscope*, *Microsc. Microanal.* **20** (2014) 1.

[19] G.F. Knoll et al., *Radiation Detection and Measurement Fourth Edition*, John Wiley & Sons Inc. (2010), pg. 124.

[20] Z. He, *Review of the Shockley-Ramo theorem and its application in semiconductor gamma-ray detectors*, *Nucl. Instrum. Meth.* **463** (2001) 250.

[21] *XCOM: Photon Cross sections Database | NIST*, http://physics.nist.gov/PhysRefData/Xcom/Text/XCOM.html.

[22] I. Kuvvetli and C. Budtz-Jørgensen, *Measurements of charge sharing effects in pixilated CZT/CdTe detectors*, *IEEE Nucl. Sci. Symp. Conf. Rec.* **3** (2007) 2252.

[23] T.E. Peterson and L.R. Furenlid, *SPECT detectors: the Anger Camera and beyond*, *Phys. Med. Biol.* **56** (2011) R145.